

Supercurrent in long ballistic graphene Josephson junctions

I. V. Borzenets^{1*}, F. Amet², C. T. Ke,³ K. Watanabe⁴, T. Taniguchi⁴, M. Yamamoto,^{1,5} S. Tarucha^{1,6}, G Finkelstein³

¹*Department of Applied Physics, University of Tokyo, Bunkyo-ku, Tokyo 113-8656, Japan*

²*Department of Physics and Astronomy, Appalachian State University, Boone, NC 28607, USA.*

³*Department of Physics, Duke University, Durham, NC 27708, USA.*

⁴*Advanced Materials Laboratory, National Institute for Materials Science, Tsukuba, 305-0044, Japan.*

⁵*PRESTO, JST, Kawaguchi-shi, Saitama 332-0012, Japan*

⁶*Center for Emergent Matter Science (CEMS), RIKEN, Wako-shi, Saitama 351-0198, Japan*

*Correspondence should be sent to I.V.B. (email: ivan@meso.t.u-tokyo.ac.jp)

We investigate the critical current I_C in Josephson junctions made of encapsulated graphene/boron-nitride heterostructures. I_C is found to scale with temperature T as $\propto e^{-k_B T/\delta E}$, which is consistent with the conventional model for ballistic Josephson junctions that are long compared to the thermal length. The extracted energy δE is independent of the carrier density and consistent with the level spacing of the ballistic cavity, as determined from Fabry-Perot oscillations of the junction normal resistance. However, δE is 2 to 2.5 times smaller than the value naively expected from the junction length. Finally, we find that at the lowest temperature, I_C saturates at a universal level determined by the product of δE and the number of modes across the junction width.

PACS numbers: 74.45.+c, 72.80.Vp, 74.50.+r, 73.23.-b

Encapsulated graphene/boron-nitride heterostructures emerged in the past year as a medium of choice for studying proximity-induced superconductivity in the ultra-clean limit [1–4]. These junctions support the ballistic propagation of superconducting currents across micron-scale graphene channels, and their critical current is gate-tunable across several orders of magnitude. In these devices, a rich phenomenology arises from the interplay of superconductivity with ballistic transport [1], cyclotron motion [2], and even the quantum Hall effect at high magnetic field [4]. However, the nature of the zero-field supercurrent in the long ballistic graphene Josephson junctions has so far not been investigated in sufficient detail.

Ballistic superconductor - normal metal - superconductor (SNS) junctions are characterized as “long” if the length of the normal region L is larger than the induced coherence length in the normal metal, $\xi = \hbar v_F/\Delta$ [5–7]. Here, Δ is the superconducting energy gap, and v_F is the Fermi velocity in the normal region. The lithographic constraints place many graphene devices in the regime $L \gtrsim \xi$. In the temperature range $\delta E \ll k_B T \ll \Delta$, where $\delta E = \frac{\hbar v_F}{2\pi L} = \frac{\xi \Delta}{2\pi L}$, the thermal averaging yields an exponential decay of the critical current: $I_C \propto \exp(-k_B T/\delta E)$. Note that δE is only dependent on the junction length L , and does not vary with the carrier density or the mobility (as long as the junction remains ballistic.) In this work, we demonstrate this exponential scaling and explore its dependence on the carrier density and the sample dimensions.

Our graphene layers are exfoliated from Kish graphite and encapsulated in hexagonal Boron-Nitride (hBN) using the “pick-up” method [8]. Heating at 250°C causes bubbles of trapped adsorbates to migrate towards the edges of the graphene mesa, effectively cleaning it. The edges of the graphene flake are exposed by etching

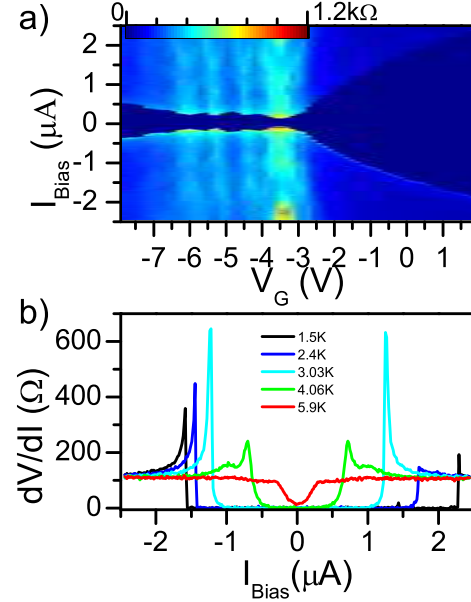


FIG. 1. a) Map of differential resistance versus current I and gate voltage V_G . The data are shown for Junction 1 and taken at a temperature $T = 1.5K$. The superconducting region of zero resistance can be observed around $I = 0$. The current through the junction is swept from negative to positive; therefore, the transition at the negative I corresponds to the retrapping current I_R , while the transition at the positive I corresponds to the switching current I_S . b) Differential resistance versus current I of Junction 1 taken at $V_G = 1V$ for different values of temperature.

through the hBN-graphene-hBN stack with a CHF_3/O_2 plasma (flow rates 40/6 sccm) at 1Pa and 60W power. The etching time varies depending on the thickness of the top hBN layer. We use DC magnetron sputtering to

form Molybdenum-Rhenium alloy contacts (50/50 wt%). These contacts are 100 – 120nm thick and are deposited at a rate of ~ 50 nm/min (with a pressure of 2 mTorr and a power of 160W [4].) This work presents data collected on three devices of varying width W and length L : Junction 1 ($L = 300$ nm, $W = 2.4\mu\text{m}$), Junction 2 ($L = 800$ nm, $W = 2.4\mu\text{m}$), and Junction 3 ($L = 650$ nm, $W = 4.5\mu\text{m}$.)

The junctions are measured in a four-terminal lock-in setup with an AC excitation current of 5 nA added on top of a variable DC bias current, I . The carrier density in graphene is controlled with a gate voltage V_G . Figure 1A presents a map of the differential resistance $dV/dI(V_G, I)$, measured on Junction 1 at $T = 1.5$ K. A supercurrent can be seen as the dark region which persists at all values of V_G . Experimentally, the current is swept from the negative to the positive values, and the transition from the normal to the superconducting state is seen in the negative region at $|I| = I_R$ (the retrapping current.) The transition from the superconducting back to the normal state happens in the positive region when $I = I_S$ (the switching current)[9]. As commonly observed in graphene Josephson junctions, the sample exhibits hysteresis, $I_S \gtrsim I_R$ [10–16], which could be attributed to either underdamped junction dynamics [9, 14], or to the self-heating by the retrapping current [16, 17]. Figure 1b shows the differential resistance of Junction 1 versus bias current I taken at $V_G = 1$ V for different temperatures. Clearly, the difference between I_S and I_R rapidly decreases with temperature, which allows to use I_S in place of the true critical current, I_C .

One can see from Figure 1b that I_C rapidly decreases with temperature. Figure 2 shows $I_C(T)$ for devices 1 and 3 plotted on a semi-log scale for several values of V_G . From here on, the gate voltage V_G is shown relative to the Dirac point. One can see that $\log(I_C)$ is linear in T over an order of magnitude [5–7], before saturating at both low and high temperatures. The slope of $\log(I_C)$ does not depend on V_G , although its value increases with the device length L . Fitting a linear dependence of $\log(I_C)$ on T yields the energy scale δE . We show two fitted curves for each junction on Figure 2 as a guide to the eye. The exponential dependence is particularly clear for the top curve in Fig. 2b, which shows the critical current ranging over more than two orders of magnitude. This temperature dependence strikingly differs from the short-junction regime observed in vertical graphene junctions, where I_C scales as $\tanh(\Delta/2k_B T)$ [6, 9, 18, 19], (with $\Delta \gg \delta E$). The exponential dependence is limited at the low temperature end, when $k_B T$ becomes comparable to δE . Indeed, the saturation is visible in Fig. 2 at $T \sim 1$ K for the shortest Junction 1, but not yet for Junction 3. In a separate cooldown, we have observed I_C saturating at lower temperatures in the longer Junctions 2 and 3.

The extracted energy δE is of the order of 0.1meV for junction 3 and 0.15 - 0.2 meV for junction 1. Figure 3a

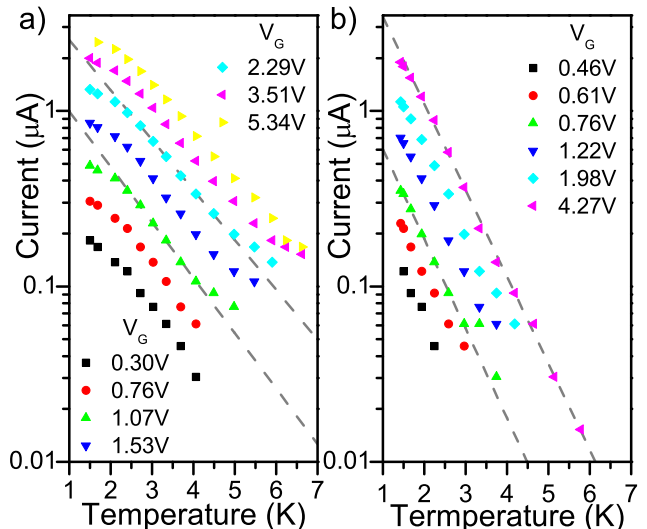


FIG. 2. Critical current I_C plotted on a semi-log scale versus temperature T for a) Junction 1 and b) Junction 3. (The values of V_G are shown relative to the Dirac point.) For a given junction, the slope of $\log(I_C)$ vs. T is independent of the gate voltage V_G . Example fits to this exponential dependence are shown as gray dashed lines. According to theory of long ballistic SNS junctions, the slope depends on the energy δE which is independent of density and is inversely proportional to the junction length L . Indeed, the longer Junction 3 exhibits a steeper slope compared to the shorter Junction 1.

shows that for a given device $\delta E(V_G)$ remains roughly constant as a function of V_G across both the electron and hole-doped regimes. Such universal scaling not dependent on carrier concentration is indeed expected in the long ballistic regime. Note, however, that the energy scale δE is $\sim 2 - 2.5$ times smaller than the value $\frac{\hbar v_F}{2\pi L}$ naively expected from the length of the device. This observation cannot be attributed to a finite reflection at superconductor-graphene interface. Indeed, the fitted energy δE remains largely unchanged whether the carriers are electrons or holes, while the transmission coefficient is both carrier type- and gate-dependent.

Instead, the likely explanation involves the fact that in our junctions the length is comparable with $\xi \approx 500$ nm, and L in the definition of δE should be replaced with $L + \xi$ [20]. Numerical simulations conducted in the regime $L \approx \xi$ indicate $I_C \propto \exp(-k_B T / \delta E)$ dependence with δE suppressed by a factor of ~ 2 (Figure 3 in Ref. 21). Deriving a universal expression for δE in the $L \approx \xi$ regime remains a theoretical challenge beyond the scope of this paper.

Remarkably, ballistic graphene Josephson junctions offer a possibility to compare δE to the measured level spacing in the junction, $E_0 = \frac{\pi \hbar v_F}{L} = 2\pi^2 \delta E$. In the hole-doped regime, the reflections of ballistic charge carriers between each contact interface yields quantum in-

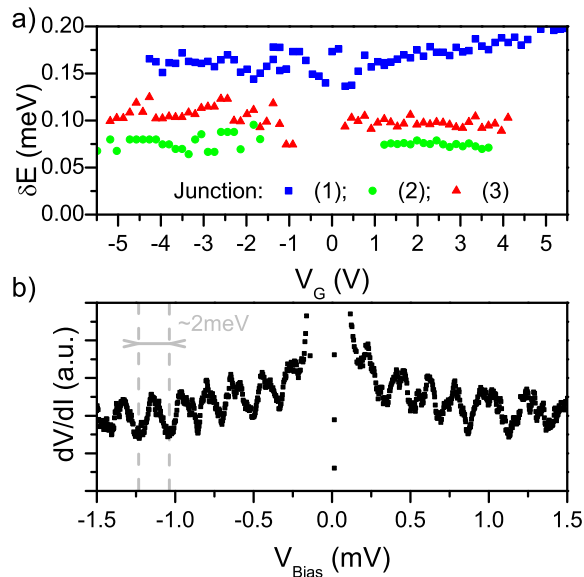


FIG. 3. (a) The gate voltage dependence of energy δE extracted from the slope of $\log(I_C)$ dependence on T . Blue \square corresponds to Junction 1, green \circ to Junction 2, and red \triangle to Junction 3. As expected, the extracted energy δE is largely independent of V_G , regardless of whether the conduction is mediated by electrons or holes. (b) Differential conductance versus bias voltage V_B for Junction 3, gated to the p-doped regime $V_G = -4.2\text{V}$. The period of these oscillations should be described by the level spacing: $E_0 = \pi\hbar v_F/L$. The extracted value of $\delta E \approx 2\text{meV}$ is consistent with the expected $E_0 = 2\pi^2\delta E \approx 20\delta E$.

terference (“Fabry-Perot”) oscillations in differential resistance dV/dI vs. bias voltage V with a period of E_0/e [2, 4, 22–24]. These oscillations are shown in Figure 3b for Junction 3 in the hole-doped regime. The oscillations have a period of approximately 2mV, which is in excellent agreement with $\delta E \approx 100\ \mu\text{eV}$ found from the $I_C(T)$ fitting.

The critical current saturates in the zero-temperature limit, which is achieved when $k_B T \ll \delta E$. In this regime, I_C should be proportional to δE : $I_C = C N e \delta E / h$, with C being a proportionality constant. Here, $N = W(4\sqrt{n/\pi})$ represents the number of transversal modes across the width W of the junction, n is the carrier density, and the factor 4 comes from the spin and valley degeneracies in graphene. Figure 4 shows the ratio $\frac{hI_C}{Ne\delta E}$ as a function of gate voltage for the electron doping, when the graphene-MoRe interfaces are highly transparent [26]. Strikingly, the curves for all three junctions are very close to each other, which strongly suggests that δE is the relevant energy scale even as $T \rightarrow 0$.

Additionally, while the ratio $\frac{hI_C}{Ne\delta E}$ is significantly reduced close to charge neutrality, it converges towards a constant (C of the order of 1) at high gate voltage. A critical current of the order of $e\delta E/h$ per transversal mode is indeed expected in the zero temperature limit[27]. The

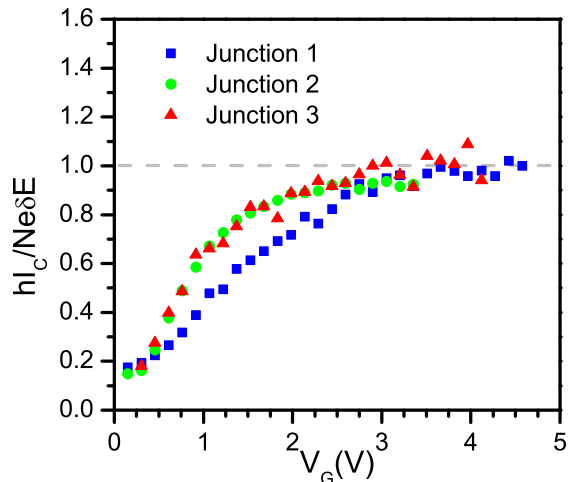


FIG. 4. Ratio $hI_C/Ne\delta E$ as a function of V_G for junctions J1, J2 and J3, measured at 40mK. The number of modes N is $W(4\sqrt{n/\pi})$, where n is the carrier density as determined from V_G . Remarkably, the plotted ratio converges toward 1 in every sample as the gate voltage increases and the transmission of the graphene-MoRe interfaces gets closer to one.

suppression of C close to the Dirac point most likely arises from the V_G dependence of the transmission coefficient τ of the superconductor-graphene interface. We extract the contact transparency from the junction normal resistance as h/Ne^2R_N and find that τ is minimal at the charge neutrality, but gets close to 1 at high densities. Accounting for τ [7, 25] makes the ratio $\frac{1}{\tau^2} \frac{hI_C}{Ne\delta E}$ constant across a wider range of V_G [28].

In conclusion, we studied the nature of the critical current in several ballistic superconductor-graphene-superconductor junctions. We observed that the critical current I_C scales with temperature as $\propto e^{-k_B T/\delta E}$. Such behavior places the samples in the long ballistic junction regime. From the slope of $\log I_C$ vs. T dependence, we extract the relevant energy parameter δE , which depends only on the junction length and is independent of the gate voltage V_G . The energy δE is 2 - 2.5 times smaller than the values naively extracted from the junction lengths, indicating the importance of the finite-length corrections. Finally, we show that at the lowest temperature, I_C saturates at a universal level determined by the product of δE and the number of transversal modes across the junction width. Our observations demonstrate the universality of the critical current in long ballistic Josephson junctions – a regime relevant to most hybrid superconductor-encapsulated graphene devices.

I. V. B. and M. Y. acknowledge the Canon foundation. C.-T. K. and G.F. were supported by the Division of Materials Sciences and Engineering, Office of Basic Energy Sciences, U.S. Department of Energy, under Award de-sc 0002765. F.A. acknowledges the ARO under

Award W911NF-14-1-0349. M.Y. acknowledges financial support by Grant-in-Aid for Scientific Research on Innovative Areas "Science of Atomic Layers". M. Y. and S. T. acknowledge support by Grant-in-Aid for Scientific Research S (No. 26220710), and Grant-in-Aid for Scientific Research A (No. 26247050). We would like to thank Konstantin Matveev for fruitful discussions.

-
- [1] V. E. Calado, S. Goswami, G. Nanda, M. Diez, A. R. Akhmerov, K. Watanabe, T. Taniguchi, T. M. Klapwijk, and L. M. K. Vandersypen, *Nature Nano.* **10**, 761-764 (2015).
- [2] M. Ben Shalom, M. J. Zhu, V. I. Fal'ko, A. Mishchenko, A. V. Kretinin, K. S. Novoselov, C. R. Woods, K. Watanabe, T. Taniguchi, A. K. Geim, and J. R. Prance, *Nature Phys.*, doi:10.1038/nphys3592 (2015).
- [3] M. T. Allen, O. Shtanko, I. C. Fulga, J. I. J. Wang, D. Nurgaliev, K. Watanabe, T. Taniguchi, A. R. Akhmerov, P. Jarillo-Herrero, L. S. Levitov, and A. Yacoby, *Nature Phys.* **12**, 128-133 (2016).
- [4] F. Amet, C. T. Ke, I. V. Borzenets, Y. Wang, K. Watanabe, T. Taniguchi, R. S. Deacon, M. Yamamoto, Y. Bomze, S. Tarucha, and Finkelstein, arXiv:1512.09083 (2015).
- [5] I.O. Kulik, *Sov. Phys. JETP* **30**, 944 (1970).
- [6] A. V. Svidzinskii, *Spacially-Inhomogeneous Problems of Theory of Superconductivity* (Nauka, Moscow, 1982).
- [7] A. A. Golubov, M. Yu. Kupriyanov, and E. Ilichev, *Rev. Mod. Phys.* **76**, 411 (2004).
- [8] L. Wang, I. Meric, P. Y. Huang, Q. Gao, Y. Gao, H. Tran, T. Taniguchi, K. Watanabe, L. M. Campos, D. A. Muller, J. Guo, P. Kim, J. Hone, K. L. Shepard, and C. R. Dean, *Science* **342**, 614-617 (2014).
- [9] M. Tinkham, *Introduction To Superconductivity* (McGraw-Hill, New York, 1996).
- [10] H. B. Heersche, P. Jarillo-Herrero, J. B. Oostinga, L. M. K. Vandersypen, and A. F. Morpurgo, *Nature* **446**, 56 (2007).
- [11] F. Miao, S. Wijeratne, Y. Zhang, U. C. Coskun, W. Bao, and C. N. Lau, *Science* **446**, 1530 (2007).
- [12] X. Du, I. Skachko, and E. Y. Andrei, *Phys. Rev. B* **77**, 184507 (2007).
- [13] C. Ojeda-Aristizabal, M. Ferrier, S. Guéron, and H. Bouchiat, *Phys. Rev. B* **79**, 165436 (2009).
- [14] I. V. Borzenets, U. C. Coskun, S. J. Jones, and G. Finkelstein, *Phys. Rev. Lett.* **107**, 137005 (2011).
- [15] I. V. Borzenets, U. C. Coskun, S. J. Jones, and G. Finkelstein, *IEEE Trans. Appl. Supercond.* **22**, 1800104 (2012).
- [16] I.V. Borzenets, U.C. Coskun, H.T. Mebrahtu, Yu.V. Bomze, A.I. Smirnov, and G. Finkelstein, *Phys. Rev. Lett.* **111**, 027001 (2013).
- [17] H. Courtois, M. Meschke, J. T. Peltonen, and J. P. Pekola, *Phys. Rev. Lett.* **101**, 067002 (2008).
- [18] M. Titov and C. W. J. Beenakker, *Phys. Rev. B* **74**, 041401(R) (2006).
- [19] G.-H. Lee, S. Kim, S.-H. Jhi, and H.-J. Lee, *Nature Commun.* **6**, 6181 (2015).
- [20] P. F. Bagwell, *Phys. Rev. B* **46**, 12573-12586 (1992).
- [21] I. Hagymasi, A. Kormanyos, and J. Cserti, *Phys. Rev. B* **82**, 134516 (2010).
- [22] V. Cheianov and V. I. Falko, *Phys. Rev. B* **74**, 041403 (2006).
- [23] F. Miao, S. Wijeratne, Y. Zhang, U. C. Coskun, W. Bao, and C. N. Lau, *Science* **317**, 15301533 (2007).
- [24] P. Rickhaus, R. Maurand, M.-H. Liu, M. Weiss, K. Richter, and C. Schnenberger, *Nature Commun.* **4**, 2342 (2013).
- [25] M. Yu. Kupriyanov and V. F. Lukichev, *Zh. Eksp. Teor. Fiz.* **94**, 139-149 (1988).
- [26] The carrier density is calculated as $n = V_G C_G / e$ is the carrier density. $C_G \approx 11.5nF$ is the gate capacitance. And V_G is counted from the Dirac point which is assumed to be the point where R_N is highest.
- [27] C. Ishii, *Prog. Theor. Phys.* **44**, 1525 (1970).
- [28] See Supplementary Information

Supplementary Information

TRANSMISSION COEFFICIENT τ AND IDEAL RESISTANCE R_{SH} V.S. MEASURED R_N

For a device governed by ballistic transport the semiclassical limit of resistance, known as the Sharvin resistance R_{SH} , is simply the inverse of the conductance through M ballistic channels, each contributing a conductivity of h/e^2 ; i.e.: $1/R_{SH} = 4Me^2/h$. (The factor 4 accounts for spin and valley degeneracy in graphene.) We calculate the number of modes M for each value of gate V_G : $M = \sqrt{\frac{1}{\pi}nW}$. Where $n = V_G C_G/e$ is the carrier density. ($C_G \approx 11.5nF$ is the gate capacitance.) In a real device, the measured resistance R_N (Figure S1a) is always higher than the ideal resistance R_{SH} due to imperfect contact interface. That is, the transmission across the superconductor-graphene interface is not unity. The transmission coefficient τ due to the contact interface can be found by comparing the measured resistance R_N to the ideal: $\tau = R_{SH}/R_N$. Taking the peak in measured resistance R_N (Figure S1a) as the Dirac point, we calculate the expected R_{SH} and extract a possible transmission coefficient τ for all three Junctions. Remarkably, τ saturates quickly in V_G and reaches quite high values of up to 0.9 (Figure S1b).

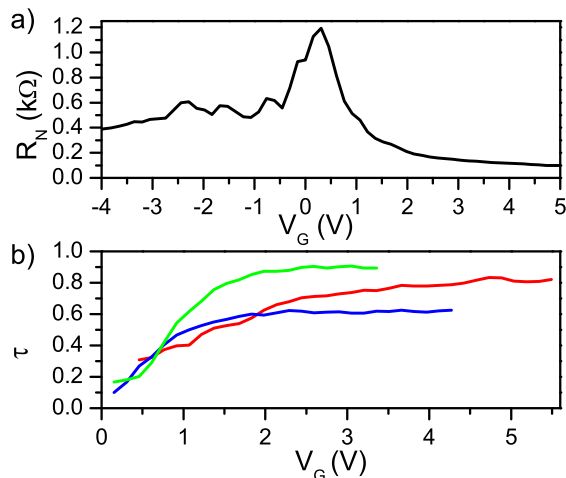


FIG. 5. a) The normal resistance R_N versus gate voltage V_G of Junction 1. In an ideal case, the normal resistance through a ballistic interface depends only on the quantum resistance scaled by the number of conducting modes M : $1/R_{SH} = 4Me^2/h$. However, the imperfect superconductor-normal interface results in non unity transmission coefficient τ which results in increased R_N . b) The calculated τ for Junction 1:(blue); 2:(green); 3:(red). τ is calculated by estimating the number of modes M from the applied gate voltage and calculating R_{SH} ; then: $\tau = R_{SH}/R_N$.

THE EFFECT OF τ ON THE I_C V.S. δE RELATIONSHIPS AT LOW T

The discussion in the main manuscript considers only the ideal long, ballistic, SNS Josephson junction in calculating the proportionality constant between I_C and δE at low temperatures (Figure 4). However, as the transmission across the superconductor-graphene interface is not perfect $\tau < 1$, a real junction effectively works as a superconductor-insulator-normal (SINIS) junction[7, 25]. For such junctions, the expected critical current is modified by the transmission. Moreover, the real resistance R_N must be used in the calculation, instead of the ideal resistance R_{SH} . In Figure S2 we plot the ratio of $eI_C R_N$ and $\tau \delta E$, taking into account the effect of imperfect transmission. Here we observe that the ratio saturates and becomes constant at gate voltages much closer to the Dirac point. However, the resulting ratio now varies slightly between devices: $\sim 1.16, 1.95, 1.5$ for Junctions 1, 2, and 3 respectively. Yet, the ratio remains remarkably close to 1 suggesting that as T approaches zero, the critical current is carried via one transversal mode per conducting channel. Such variation could come from a mis-estimation of τ originating from a wrong choice of the location of the Dirac point. Alternatively, the variation of proportionality can come from existence of impurities in the graphene. In a junction of finite length L single point impurities can couple to the Andreev energy levels, opening gaps in the quasiparticle level spectrum[20], without affecting the measurement of R_N . Note that Ref.20 is a general consideration of impurities in a ballistic channel: only considering the local scattering probability. Therefore, we can not infer anything about the nature of the impurities, such as the formation of Shiba states[?].

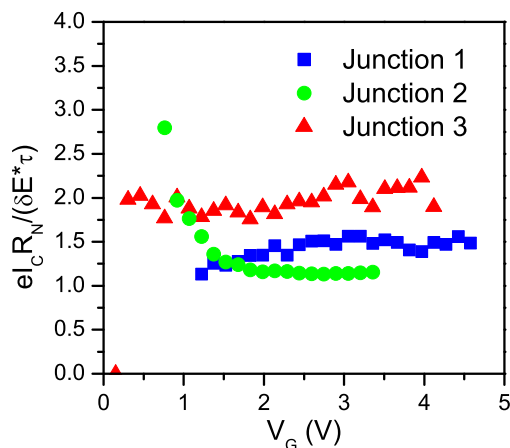


FIG. 6. The ratio $eI_C R_N / \tau \delta E$ for Junction 1 (blue \square), 2 (green \circ), 3 (red \triangle). The resulting ratio is gate independent with the proportionality constant $C \sim 1$

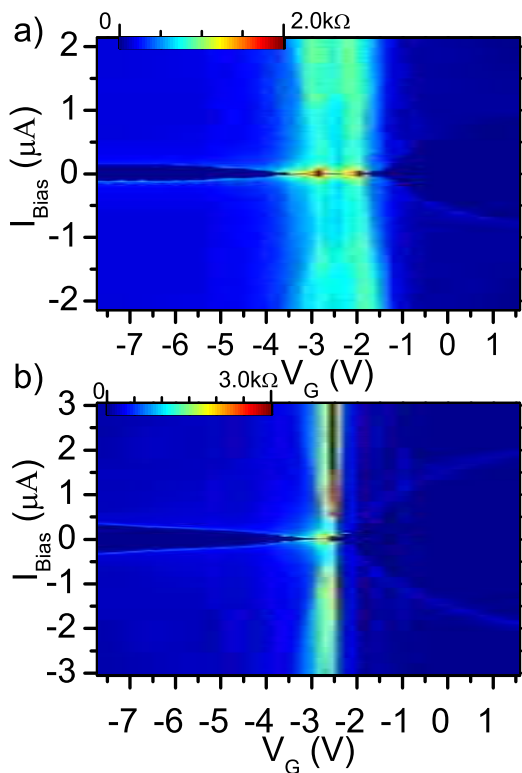


FIG. 7. Map of differential conductance versus bias current I for different values of gate voltage V_G . The data is shown for Junction 2 (a) and Junction 3 (b) taken at a temperature $T = 1.5K$. Around $I = 0$ a region of zero resistance can be observed. This superconducting region persists until I reaches a critical value. The current through the junction is swept from a large negative value to a large positive. Therefore, the transition at negative I corresponds to the retrapping current I_R , while the transition at positive I corresponds to the switching current I_S .

DIFFERENTIAL RESISTANCE $dV/dI(V_G, I)$ JUNCTIONS 2 AND 3

Figure S1 shows maps of differential conductance versus bias current and gate voltage taken at base temperature for Junction 2 and Junction 3. Both Junction 2 and 3 are significantly longer than Junction 1, hence, oscillations in the critical current I_C in the hole conduction regime are difficult to observe. Junction 2, the longest junction, features a double peak suggesting that impurities begin to play a higher role.

CRITICAL CURRENT I_C V.S. T DEPENDENCE OF JUNCTION 2

We analyze Junction 2 in the manner identical to that of Junction 1 and 3. Figure S2 shows $I_C(T)$ plotted on a semi-log scale for several values of V_G . (The gate voltage V_G is shown relative to the right-most Dirac peak.) Here, $\log(I_C)$ is linear in T over a significant range. As Junction 2 is the longest, the slope of the curves is the most steep, and the saturation temperature is the lowest resulting in a smaller available range. The slope of $\log(I_C)$ doesn't depend on V_G . Fitting a linear slope to $\log(I_C)$ yields the energy scale δE .

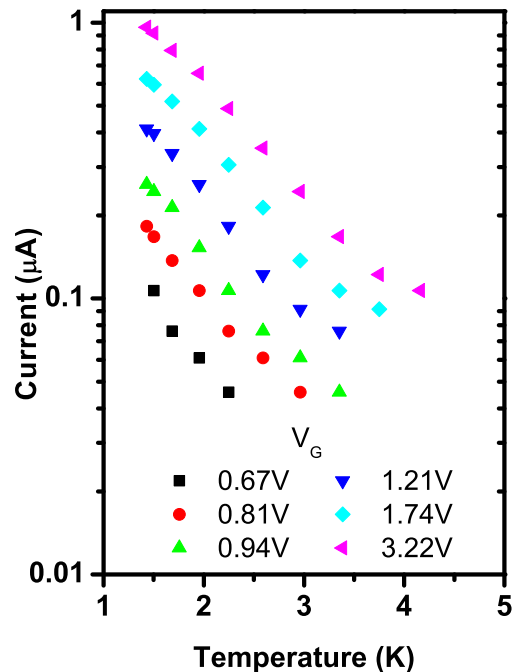


FIG. 8. Critical current I_C versus temperature T plotted on a semi-log scale for Junction 2. (V_G is shown relative to the Dirac point.) Slope of $\log(I_C)$ v.s. T is independent of gate voltage V_G .